

Heterogeneous & Homogeneous & Bio- & Nano-

CHEMCATCHEM

CATALYSIS

Accepted Article

Title: From Active Site Models to Real Catalysts: Importance of the Material Gap in the Design of Pd Catalysts for Methane Oxidation

Authors: Hieu A Doan, Munish K Sharma, William S Epling, and Lars C Grabow

This manuscript has been accepted after peer review and appears as an Accepted Article online prior to editing, proofing, and formal publication of the final Version of Record (VoR). This work is currently citable by using the Digital Object Identifier (DOI) given below. The VoR will be published online in Early View as soon as possible and may be different to this Accepted Article as a result of editing. Readers should obtain the VoR from the journal website shown below when it is published to ensure accuracy of information. The authors are responsible for the content of this Accepted Article.

To be cited as: *ChemCatChem* 10.1002/cctc.201601333

Link to VoR: <http://dx.doi.org/10.1002/cctc.201601333>

WILEY-VCH

www.chemcatchem.org



From Active Site Models to Real Catalysts: Importance of the Material Gap in the Design of Pd Catalysts for Methane Oxidation

Hieu A. Doan^[a], Munish K. Sharma^[a], William S. Epling^[a,b] and Lars C. Grabow^{*[a]}

Rapid computational screening to aid novel catalyst design has evolved into an important and ubiquitous tool in modern heterogeneous catalysis. A possible shortcoming of this approach, however, is the material gap, where simplified computational models used for catalyst screening do not always capture the complexity of real catalytic systems. Here we investigate the importance of the material gap for complete methane oxidation over supported Pd/ γ -Al₂O₃ catalysts using a combination of Density Functional Theory (DFT) simulations and Temperature Programmed Oxidation (TPO) experiments. The Pd/ γ -Al₂O₃ active site was approximated by four models of increasing complexity, namely Pd(100), Pd(211), PdO(101), and Pd₁₀/ γ -Al₂O₃(110), and each was also modified with metal promoters in order to discover

reactivity trends. Although the unpromoted Pd model surfaces exhibit different methane activation activities, our DFT results indicate that an experimentally verified performance trend can be predicted for their promoted counterparts irrespective of the active site representation. We attribute the robustness of the trend predictions in this particular system to localized changes in the electron density during methane activation. Overall, our work supports the commonly practiced active site model simplifications during computational catalyst screening and provides fundamental insight into the qualitative agreement between theory and experiment for methane oxidation over promoted Pd catalysts.

Introduction

Recent advances in density functional theory (DFT) and computing power have made computational catalyst screening a viable alternative to traditional trial-and-error experimental approaches.^[1–5] Computational screening typically reduces the number of parameters that describe catalytic behaviors in terms of activity and selectivity to a few energy descriptors that can be easily calculated from DFT. This reduction in complexity to the descriptor-based method is achieved through scaling relationships, which relate the energy of intermediates and transition states to the adsorption energies of a small set of intermediates that serve as descriptors.^[6–10]

Although heterogeneous catalysts have complex or even multiple active sites, computational catalyst screening approaches routinely assume that simplified active site representations, such as fcc(100), fcc(111) or fcc(211) facets, are sufficiently accurate to obtain reliable catalytic trends at maximized computational efficiency. Although such simplification definitely affects the absolute values and quantitative outcomes, trend predictions are assumed to be independent of the material gap between oversimplified computational model systems and real catalyst surfaces. Yet, other than anecdotal evidence, there has not been a systematic study questioning the validity of this

assumption. Given the success and increasing popularity of computational catalyst screening,^[11,12] the important question regarding the role of the material gap remains: is it always necessary to close the material gap by using increasingly complex catalyst models to predict qualitative reactivity, and more importantly, selectivity trends, or is the current practice and use of simplified models sufficient in certain cases?

In this study, we attempt to answer the above question by investigating the importance of the material gap in catalytic trend studies for complete methane oxidation over Pd/ γ -Al₂O₃ catalysts using a combination of DFT calculations and temperature programmed oxidation (TPO) experiments. This catalytic system is a good benchmark because the reaction is structure-sensitive,^[13,14] the activity depends on the oxidation state of Pd in response to the reaction environment,^[15–18] and the choice of support affects catalytic performance.^[19] Furthermore, methane combustion catalysis is of practical importance as unburnt methane slip from natural gas vehicles contributes to detrimental greenhouse gas emissions. To examine the effects of the material gap, we approximated the Pd/ γ -Al₂O₃ active site with four popular computational models of increasing complexity: Pd(100), Pd(211) PdO(101), and Pd₁₀/ γ -Al₂O₃(110). Among these, Pd(100) and Pd(211) distinguish between terrace and step sites, respectively, of a metallic Pd catalyst nanoparticle. Pd(100) was chosen over Pd(111) to represent the terrace site, because methane activation was shown to be noticeably more favorable on the former^[20] and the active oxide phase of Pd, PdO, was suggested to preferentially form on the less packed Pd(100) than the dense hexagonal Pd(111).^[21] The PdO(101) thin film, on the other hand, has been shown to be the most stable termination that grows epitaxially on Pd(100)^[22] or Pd(111)^[23] under oxidizing conditions. Since the structure and activity of PdO(101) thin film do not deviate much from those of bulk-terminated PdO(101),^[20,23] the latter model was employed in this study. The more complex

[a] Hieu A. Doan, Munish K. Sharma, William S. Epling and Lars C. Grabow
Department of Chemical and Biomolecular Engineering
University of Houston
Houston, TX 77204-4004, USA
E-mail: grabow@uh.edu

[b] William S. Epling
Department of Chemical Engineering
University of Virginia
Charlottesville, VA 22904-4741, USA

Supporting information for this article is given via a link at the end of the document.

FULL PAPER

$\text{Pd}_{10}/\gamma\text{-Al}_2\text{O}_3(110)$ model, which consists of a 10-atom Pd nanocluster supported on $\gamma\text{-Al}_2\text{O}_3$, was used to represent the metal/support interface. To define a tractable problem scope we limit our study to reaction conditions, under which the unimolecular CH_4 activation reaction is rate-limiting,^[24] and we consider only $\gamma\text{-Al}_2\text{O}_3$ as support, which is not expected to actively participate, but only indirectly alter the properties of the supported metal nanoparticle. Furthermore, in order to predict reactivity trends for each active site representation, we modified each active site model with cobalt (Co), copper (Cu), nickel (Ni), and platinum (Pt) metal promoters under consideration of their thermodynamic most favorable substitution site.

Results and Discussion

Methane activation was first investigated on un-promoted Pd and PdO surface models, which are considered reference systems. Figure 1 shows transition state geometries as well as activation energy barriers (E_a) associated with methane activation on pure PdO(101), Pd(100), Pd(211) and $\text{Pd}_{10}/\gamma\text{-Al}_2\text{O}_3$. The E_a values obtained for Pd(100), Pd(211) and PdO(101) are in good agreement with previously reported data.^[20,25] As shown in Figure 1, the calculated activation barriers depend on the catalyst models and the material gap certainly influences their absolute magnitudes. Among our investigated systems, the terrace model, Pd(100), activates methane with the highest energy barrier of 0.78 eV, whereas methane activation on the supported $\text{Pd}_{10}/\gamma\text{-Al}_2\text{O}_3$ requires an energy barrier of only 0.55 eV. For Pd(100), Pd(211), and PdO(101) surfaces, methane was found to adsorb weakly ($E_{ads} \sim -0.1$ eV); hence, the expected activation mechanism is dissociative adsorption of methane gas ($\text{CH}_4(\text{g}) + 2^* \rightarrow \text{CH}_3^* + \text{H}^*$, where * represents an unoccupied Pd site). On the other hand, methane adsorption is stronger on $\text{Pd}_{10}/\gamma\text{-Al}_2\text{O}_3$ ($E_{ads} = -0.21$ eV), which may indicate adsorption and pre-activation of methane molecules prior to H-CH₃ bond cleavage ($\text{CH}_4(\text{g}) + 2^* \rightarrow \text{CH}_4^* + ^* \rightarrow \text{CH}_3^* + \text{H}^*$). Indeed, methane adsorbed on $\text{Pd}_{10}/\gamma\text{-Al}_2\text{O}_3$ is distorted with a noticeably larger H-C-H bond angle ($\angle 114^\circ$) for H atoms close to the surface, compared to that on Pd(100) ($\angle 111^\circ$) and any H-C-H angle of the methane gas molecule ($\angle 109.5^\circ$). In the final state after CH_4 dissociation the resulting methyl (CH_3) group preferentially binds on top of a (low-coordinated) Pd atom for all surface models, but the final position of the H atom differs. Specifically, bridge or hollow sites serve as hydrogen abstraction

sites on metallic systems (Figure 1b-d), whereas lattice oxygen (O_{lat}) accepts the H atom in PdO(101) (Figure 1a). For our most complex catalyst model, $\text{Pd}_{10}/\gamma\text{-Al}_2\text{O}_3$ that represents the metal/support interface, the d -band center calculations show that the most active Pd atoms, i.e., those with the highest d -band center, are not the interfacial ones, but the metallic Pd atoms away from the interface (Figure S1). Indeed, subsequent NEB calculations confirmed that the methane activation energy barrier at Pd sites away from the interface is about 1.0 eV smaller than the energy barrier required for the same process at the interface (1.64 eV vs. 0.55 eV). These results are consistent with the previous study by Baldwin and Burch, which concluded that alumina supports only affect methane oxidation activity indirectly by altering the morphology of Pd nanoparticles.^[26]

The promoted Pd and PdO surfaces were created by replacing a surface Pd atom with a metal promoter within one unit cell (see Methods and Table S1 for more details). Such a replacement scheme translates to a ca. 3:1 ratio of Pd to promoter in the uppermost layer of the surface. As shown in Figure 1, methane preferentially activates on top of a Pd atom on the un-promoted surfaces. Thus, we considered two distinct pathways for methane activation on promoted systems and differentiated between $\text{CH}_3\text{-H}$ bond cleavage over either a Pd or the promoter atom. The first pathway results in the methyl group bound to a Pd atom, whereas the methyl group bonds to the promoter in the second pathway. Although both pathways were examined for methane activation on all promoted systems, only E_a values associated with the more favorable pathway are reported here. A summary of these results is shown in Figure 2, showing the methane activation energy barrier (ordinate) calculated for four Pd surface models promoted with Co ($\text{Co}_{\text{pr}}\text{Pd}$), Cu ($\text{Cu}_{\text{pr}}\text{Pd}$), Ni ($\text{Ni}_{\text{pr}}\text{Pd}$) and Pt ($\text{Pt}_{\text{pr}}\text{Pd}$) (abscissa). The data points for Pd (red) correspond to the E_a values of the un-promoted systems reported earlier in Figure 1 and serve as references. With the Cu promoted systems being an exception, the most interesting feature in Figure 2 is the consistent trend in promoted activity across all surface models. For example, Pt (blue) and Ni (green) promoted systems always show higher activities (lower activation energy barriers) than those of the pure surfaces. In contrast, the presence of Co (purple) leads to the highest activation energy barrier, or lowest activity, regardless of the surface model. Besides the notable agreement in the qualitative trend across all models, quantitative discrepancies are also apparent. The larger range of calculated activation energy barriers of the low-coordinated Pd surfaces, i.e.

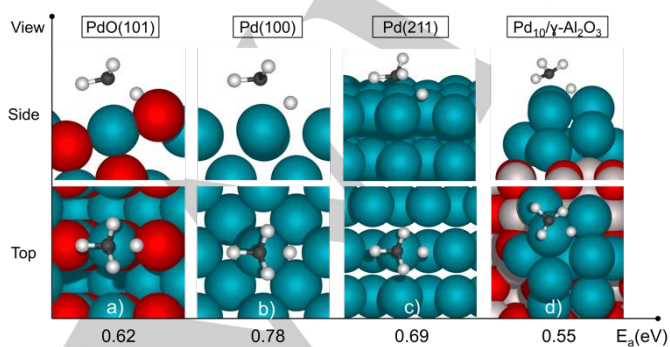


Figure 1. Transition state geometries and calculated energy barriers for methane activation on (a) PdO and (b-d) Pd catalyst models. Atomic color codes: blue (Pd), red (O), grey (Al), black (C) and white (H).

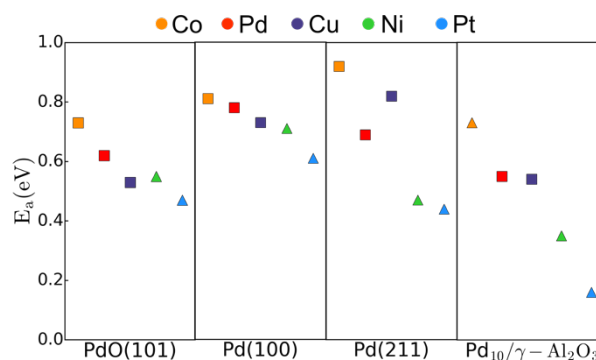


Figure 2. Calculated energy barriers for methane activation (in eV) on pure and promoted surface models of Pd and PdO catalysts. Squares and triangles indicate activation pathways over Pd or the promoter atom, respectively.

FULL PAPER

Pd(211) (coordination number, $cn = 7$) and $\text{Pd}_{10}/\gamma\text{-Al}_2\text{O}_3$ ($cn = 5$), compared to the terrace Pd(100) ($cn = 8$) suggests a stronger promotional or inhibitive effect. By comparing the slopes of Figure 2b-d, we may conclude that the lower the coordination of the Pd surface is, the larger the extent of promotion will be. Again, the sensitivity of the absolute values for methane activation on modified Pd and PdO surfaces speaks to the existence of structure sensitivity and the material gap. In particular, these results indicate that the effect of promoters is not only electronic, but also geometric in nature. Nevertheless, all models are equally reliable when differentiating between activity promoters and inhibitors.

of Cu atoms may be responsible for this phenomenon. Indeed, our DFT results indicate that Cu substitution is ca. 0.1 eV more stable on the lower coordinated Pd(211) step site than on the Pd(100) terrace. Therefore, it is plausible that Cu atoms migrate from high to low coordinated surface sites, or even between the bulk and surface of nanoparticles^[28] after every cycle, and eventually reduce the catalyst activity. The data in Figure 2 shows that the effect of Cu depends on the structural model of the catalyst site and is consistent with this interpretation. Other phenomena such as sintering or inhibition by H_2O may also contribute, but a detailed investigation of the deactivation mechanism is outside the scope of this study.

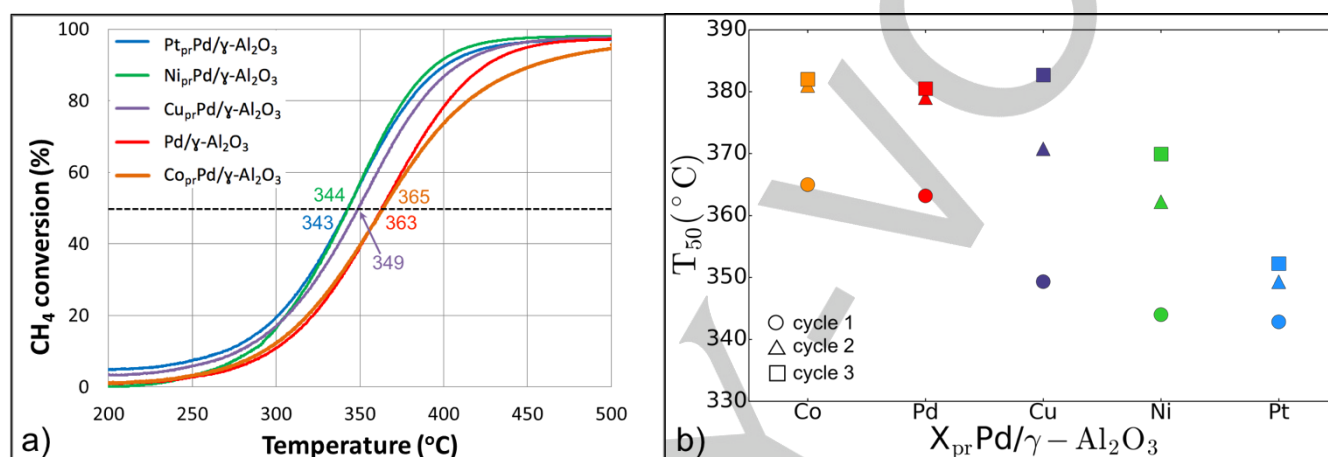


Figure 3. Temperature programmed oxidation of methane on pure and promoted Pd/γ-Al₂O₃ catalysts. a) Effects of promoters on methane combustion light-off curves and T₅₀ values (where the black dashed line intersects) during the first cycle. b) T₅₀ values of methane combustion over three cycles (0.2% CH₄, 6.0% O₂, N₂ balance, heating/cooling rate 5°C min⁻¹). T₅₀ value indicates the temperature at which methane conversion reaches 50%.

Temperature programmed oxidation (TPO) tests were conducted to compare CH₄ oxidation activities over a series of pure and promoted Pd/γ-Al₂O₃ catalyst samples. Three heating-cooling cycles and T₅₀ (°C) values, i.e. the temperature when methane conversion reaches 50%, were measured. A 0.2 vol% CH₄, 6 vol% O₂, and balance N₂ feed composition was used, for which the activation of methane is known to be rate-limiting.^[13] Additional information is provided in the Methods section. Figure 3a shows light-off curves and lists the T₅₀ for each catalyst for the first cycle. The T₅₀ values show a consistent trend with activation barrier estimates using TPO data below 20 % conversion, which are given in Figure S2. A complete summary of the T₅₀ (°C) values, which are indicative of catalytic activity, is given in Figure 3b for all three cycles. The relative order of the overall promotional effect extracted from Figure 3 is Pt > Ni > Cu > Co and is identical to our theoretical predictions. Certainly, Pt stands out as the best methane oxidation promoter, and the consistent activity of the Pt-promoted catalyst for all cycles suggests that Pt also reduces catalyst deactivation. Ni also enhanced the activity over all three cycles, and the addition of Co consistently leads to lower methane oxidation activity. For Cu-substituted systems, the experimental results do not follow such a consistent trend, since Cu acts as a promoter in the first two cycles (decreased T₅₀), and as a weak inhibitor in the third cycle (increased T₅₀). In the past, a Cu-Pd alloy has been shown unfavorable for methane combustion over Pd-Cu/SiO₂ catalysts, where increasing the Cu loading led to a decrease in activity.^[27] Since the Cu content in our catalyst remains constant over three cycles, we speculate that the mobility

Results obtained from our computational and experimental study exhibit a consistent trend for metal promoters. The trend is largely independent of the computational model representation of the active site, but the extent of promotion is affected by the model choice. Notably, theory and experiment both show that Pt-promoted Pd catalysts are superior for methane oxidation.

Table 1. Calculated dipole moments of CH₄ in the transition states of methane activation on Pd(100), Pd(211), PdO(101), and Pd/γ-Al₂O₃ surfaces.

Promoter	$\mu^{TS} (e \times \text{\AA})$			
	PdO(101)	Pd(100)	Pd(211)	Pd ₁₀ /γ-Al ₂ O ₃
Pt	0.25	0.23	0.25	0.36
Ni	0.17	0.12	0.13	0.12
Cu	0.19	0.13	0.13	0.15
Pd	0.21	0.14	0.13	0.12
Co	0.18	0.14	0.14	0.17

In order to explain why the active site geometry influences the magnitude, but not the direction of promotion/inhibition, we examine the C-H bond breaking transition state more closely. For methane activation over similar metallic systems such as Ni(100) and Ni(111), Bengaard and co-workers showed that the activation energy barriers are largely influenced by the electrostatic interactions between CH₄ and these surfaces.^[29] Hence, dipole moments (in the direction perpendicular to the surface) of

FULL PAPER

methane in the transition state, μ^{TS} , on the systems of interest were calculated with DFT and summarized in Table 1.

As shown in Table 1, pure metallic Pd(100), Pd(211), and Pd/ γ -Al₂O₃ surfaces seem to polarize the transition state of CH₄ equally with μ^{TS} values of 0.14, 0.13, and 0.12 (e \times Å), respectively. For PdO(101), however, the induced dipole moment on the methane activation transition state is significantly larger. Considering the fact that the calculated activation barrier on PdO(101) lies between the barrier for Pd(211) and Pd₁₀/ γ -Al₂O₃, we can conclude that the dipole moments in Table 1 cannot be directly related to the corresponding activation barriers. Moreover, Ni, Cu and Co-promoted Pd systems produce similar dipole moments of methane in the transition state compared their unpromoted counter parts, yet differences in activation barriers exist. When Pt is used as the promoter, however, the magnitudes of μ^{TS} for promoted and pure systems show considerable differences. Interestingly, when the change in activation energy barrier is plotted against the change in dipole moment for Pt-promoted surfaces (Figure 4), two observations can be made. First, the promoting effect of Pt differs across all surface models, with the supported Pd₁₀/ γ -Al₂O₃ system having the most significant improvement and largest dipole change. Furthermore, since the ratio of Pt to Pd is similar on all promoted surfaces, the variance in activity gain must primarily come from geometric effects. Second, the straight line with a slope of ca. -1.32 and x-intercept of -0.08 eV indicates a linear relationship between the enhancement in activity (measured by the change in activation energy barrier) and the dipole moment induced by Pt atoms. A simple rule of thumb that can be deduced from this relationship is that the activation energy barrier is lowered by 1.32 eV for every e \times Å gained in the dipole moment of methane in the transition state on Pt_{pr}Pd surfaces.

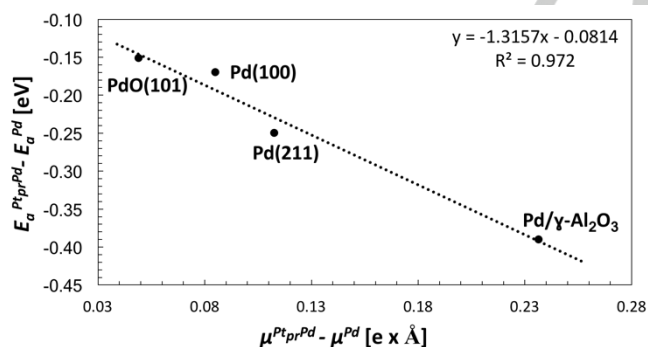


Figure 4. Gain in activity (measured as decrease in energy barrier) as a function of change in transition state dipole moment of methane on Pt_{pr}Pd surfaces.

Although electrostatic interactions, as quantified by surface-induced dipole moments in the transition state of methane activation, can provide some possible explanation for the promoting effects of Pt on Pd catalysts, they do not capture the consistent promotional or inhibitive effects of the other metal modifiers, namely Ni, Cu, and Co. Since the transition state dipole moments discussed so far result from a projection of charge density distribution changes onto the surface normal, we further investigated the full charge density difference to gain more insights into the transition state of methane activation. In particular, the full charge density difference map for methane activation on modified Pd(100) surfaces is shown in Figure 5.

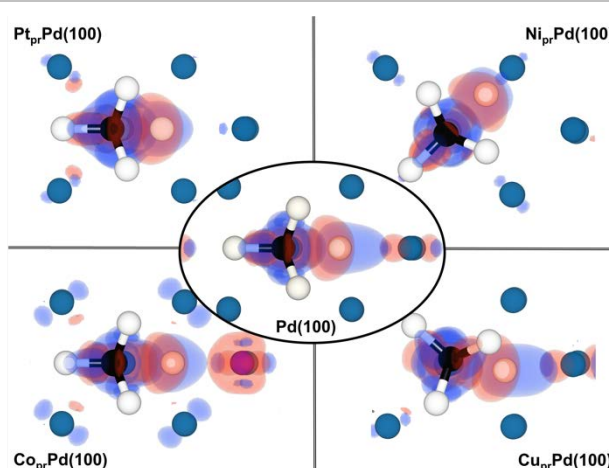


Figure 5. Charge density difference for the transition states of methane activation (top view) on pure and promoted Pd(100) surfaces. The promoter atoms on Pt_{pr}Pd(100) and Ni_{pr}Pd(100) surfaces are directly underneath the methyl group, while Co in Co_{pr}Pd(100) accepts the H atom. The Cu atom in Cu_{pr}Pd(100) is further away and not visible in the inset (See Table S1 for more details). Red/blue indicates charge depletion/accumulation. Atomic color code C = black, H = white, Pd = blue, and Co = magenta.

The H-CH₃ bond cleavage transition state on pure Pd(100) is characterized by charge depletion between CH₃ and H (red area) and charge accumulation between H and the surface (blue area). While these features are also present on the modified Pd(100) systems, their distribution differs from one surface to another. According to Figure 5, the charge density difference isosurface for Pt_{pr}Pd(100) is confined around the Pt atom at which CH₄ binds to the surface. On the other hand, the same isosurface is more delocalized on the Co-promoted Pd(100) system.

By visual inspection, one can rank Pd(100) surfaces in terms of the spatial extent of charge density difference distribution in the following ascending order: Pt_{pr}Pd(100) < Ni_{pr}Pd(100) < Cu_{pr}Pd(100) < Co_{pr}Pd(100). Since this is the same order we obtained for DFT-derived activation energy barriers (Figure 2) or experimental T₅₀ values (Figure 3), we propose that the localization of charge density changes in the transition state, rather than the dipole moment projected onto the surface normal, is responsible for the improvement in catalytic activity. Assuming that charge is redistributed to cause a similar potential difference $\Delta\phi$ over a shorter distance d , then the C-H bond is subject to a stronger local electric field E , which can be approximated as $E = -\Delta\phi/d$. This stronger local electric field aids in the C-H scission step and suggests that electrochemical routes with controllable field effects combined with thermal activation are promising approaches for selective CH₄ conversion.^[30] This argument is in agreement with calculations shown in Figure S3 for Pd(100), Co_{pr}Pd(100), and Pt_{pr}Pd(100) in the presence of an externally applied field. The Pt_{pr}Pd(100) system with the strongest local field exhibits the highest sensitivity to changes in an externally applied field. Furthermore, as the promoted transition states are more confined, they become less sensitive to the geometric arrangement and property of the surrounding atoms. Hence, we speculate that the localization of the transition state charge density changes contributes to the robustness of the activity trend predictions across promoted model systems of varied complexity.

FULL PAPER

Conclusions

In conclusion, the activity of a series of promoted Pd catalysts for methane activation has been investigated with DFT calculations and TPO experiments. Four active site representations of varied complexity were evaluated. DFT calculations predict a consistent trend for metal modification and identified Pt as the best promoter regardless of the surface model. TPO experiments performed on promoted Pd/ γ -Al₂O₃ catalysts yield the same activity trend as predicted by DFT. The strong promotional effect of Pt was attributed to a strong electrostatic interaction between methane in the transition state and the Pt promoted surface. In general, we propose that the localization of charge density changes is ultimately responsible for promoting or inhibiting CH₄ activation on Pd-based catalysts. Furthermore, the confined charge density distribution in the transition state of methane activation contributes to the robustness of the predicted trend of promoter efficacy. Overall, this work supports the common use of simplified active site models for computational catalyst screening of reaction systems with negligible metal/support interaction, and a well-defined, unimolecular rate-determining step with a localized transition state.

Methods

Density functional theory

Periodic density functional theory (DFT) calculations were performed using the Vienna ab-initio simulation package (VASP)^[31–34] and the python modeling interface provided by the atomic simulation environment (ASE).^[35] The core and valence electrons were represented by the projected augmented wave (PAW) method^[36,37] with a kinetic energy cut-off of 400 eV. Exchange and correlation were described by the Perdew-Wang (GGA-PW91) functional.^[38] Gaussian smearing with Fermi temperatures of $k_b T = 0.1$ eV was employed and the total energies were subsequently extrapolated to $k_b T = 0.0$ eV.^[39] For geometry optimizations, forces were converged below 0.05 eV/Å.

The Pd(100) and PdO(101) surfaces were modeled as slabs with a (2x2) unit cell, whereas slabs with a (2x1) unit cell were employed for the stepped Pd(211) surface. Each slab consists of an equivalent of four layers in which the top two were allowed to relax and the bottom two were fixed to their bulk positions. The Brillouin zone for these systems was sampled using a 6 × 6 × 1 Monkhorst-Pack k-point set.^[40] The calculated lattice constants are $a = 3.958$ Å for Pd and $a = 3.100$ Å and $c/a = 1.755$ for PdO. The Pd/ γ -Al₂O₃ interface was represented by a 10-atom Pd cluster connected to the γ -Al₂O₃(110) support via its largest (111) facet. The γ -Al₂O₃(110) surface was cleaved from Digne's γ -Al₂O₃ model^[41] to make a three-layer slab with a (2x2) unit cell, where the top layer was relaxed and the bottom two layers were fixed in their bulk position. The calculated lattice parameters for bulk γ -Al₂O₃ are $a = 5.577$ Å, $b/a = 1.506$, $c/a = 1.447$, $\alpha = \gamma = 90^\circ$ and $\beta = 90.54^\circ$, and in good agreement with the previous works of Digne^[41] and Wang.^[42] All slabs were separated with a vacuum of 14 Å along the normal direction to the surface. A dipole correction to the electrostatic potential^[43] was included to separate adjacent unit cell images. Gaussian smearing with Fermi temperature of 0.01 eV was employed and the total energies were subsequently extrapolated to $k_b T = 0.0$ eV.^[39]

The promoted systems were created by replacing surface Pd atoms, one at a time, with a promoter and allowed to relax to their optimized geometries. On the Pd(100) surface one of the identical terrace atoms was replaced, while for Pd(211) an undercoordinated step atom was substituted. For PdO(101), there are two types of Pd atoms: one coordinated with four oxygen atoms and the other coordinated with only three oxygen atoms; both were considered for substitution. For the Pd₁₀/ γ -

Al₂O₃ system, both interfacial and low-coordinated Pd atoms away from the interface are important, and the most active atom of each type, according to *d*-band center calculations, was promoted.

Gas phase methane molecules were calculated in a cubic box of 10³ Å³, and the Brillouin zone was sampled at the Gamma point.^[40] Adsorption energies for CH₄ (E_{ads}) are provided with reference to the corresponding relaxed surfaces and the gas-phase species CH₄. Activation energy barriers (E_a) were calculated using the climbing image nudged elastic band (CI-NEB) method^[44] and all transition states were confirmed via vibrational analysis, showing a single imaginary mode along the reaction pathway.

Catalyst preparation

Pure Pd (1 wt%) catalysts and Pd catalysts doped with a second metal (0.4 wt%) were prepared using the incipient wetness impregnation method. The catalysts were prepared using impregnation of metal salt precursors on γ -Al₂O₃ (high purity activated alumina Al₂O₃, Puralox TH 100/150 Sasol Germany GmbH). The γ -Al₂O₃ has a packed bulk density of 700-950 (g/l), particle size $D_{50} = 40$ μm, pore volume = 0.8-1 (ml/g), pore radius=11 nm, surface area = 20 m²/g. The metal precursors used were water soluble nitrate salts such as palladium (II) nitrate dihydrate Pd(NO₃)₂·2H₂O (Aldrich, 40% metal basis), tetraammineplatinum (II) nitrate Pt(NH₃)₄(NO₃)₂ (Aldrich, 99.99 % trace metal basis), nickel (II) nitrate hexahydrate Ni(NO₃)₂·6H₂O (Aldrich, 99.99 % trace metal basis), copper (II) nitrate hydrate Cu(NO₃)₂·xH₂O (Aldrich, 99.99 % trace metal basis), cobalt (II) nitrate hexahydrate Co(NO₃)₂·6H₂O (Aldrich, 99.99 % trace metal basis). All promoted catalysts were prepared using co-impregnation, the Pd and dopant metal atoms were both present in solution. Excess water was removed from the samples through overnight heating at 100°C. The final calcination step was a 550 °C exposure in air, held for 5 hrs. Calcined catalysts were sieved to 40/60 mesh size. Silica beads with similar size were mixed with the catalyst particles to form the catalyst bed. Glass wool was used to hold the particles in place. A K-type thermocouple (Omega Engineering, Inc.) was placed at the middle of the bed.

Catalysts testing

Catalytic tests were carried out in a quartz tube reactor at atmospheric pressure. A catalyst weight of 29.3 mg was used with a total gas flow rate of 200 mL/min. The gas hourly space velocity (GHSV) for all the experiments was fixed at 50,000 hr⁻¹ (this is based on monolith loading of 2 g/inch³). The feed gas composition was 0.2 vol% CH₄, 6 vol% O₂, and balance N₂. The TPO experiments consisted of three cycles, where the temperature was ramped up and down between 25°C to 500°C at a heating/cooling rate of 5 °C /min using a Thermo Scientific, Lindberg Blue Mini-Mite tube furnace. A pretreatment in 6 vol% O₂ and balance N₂ (total gas flow rate of 200 mL/min) at 500 °C for 1 hr (heating/cooling rate of 5 °C /min) was done before recording the first light-off curve. The CH₄ and CO₂ compositions were measured at the outlet of reactor using a Pfeiffer OMNI^{star} mass spectrometer.

Acknowledgements

The authors acknowledge Shell Oil Company for financial support. LCG also acknowledges the NSF CAREER award number 1454384. Computational resources were provided by the uHPC cluster managed by the University of Houston and acquired through NSF award number 1531814. This work used the Extreme Science and Engineering Discovery Environment (XSEDE), which is supported by National Science Foundation grant number ACI-1053575, and HPC resources provided by the Texas Advanced Computing Center (TACC) at The University of Texas at Austin. We also acknowledge the use of computational

FULL PAPER

resources provided by the National Energy Research Scientific Computing (NERSC) Center, a DOE Office of Science User Facility supported by the Office of Science of the U.S. Department of Energy under contract number DE-AC02-05CH11231. Use of the computational resources at the Center for Nanoscale Materials, an Office of Science user facility, was supported by the U.S. DOE, Office of Science, Office of Basic Energy Sciences, under contract number DE-AC02-06CH11357. Finally, we thank the Center of Advanced Computing and Data Systems (CACDS) at the University of Houston for access to the Maxwell/Opuntia HPC clusters.

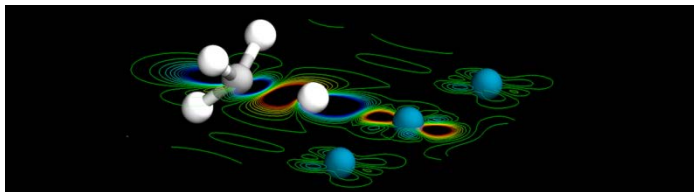
Keywords: Material gap • Methane oxidation • Palladium catalysis • Density Functional Theory • Temperature programmed oxidation

- [1] M. Andersson, T. Bligaard, A. Kustov, K. Larsen, J. Greeley, T. Johannessen, C. Christensen, J. K. Nørskov, *J. Catal.* **2006**, *239*, 501–506.
- [2] J. K. Nørskov, T. Bligaard, J. Rossmeisl, C. H. Christensen, *Nat. Chem.* **2009**, *1*, 37–46.
- [3] F. R. Negreiros, E. Aprà, G. Barcaro, L. Sementa, S. Vajda, A. Fortunelli, *Nanoscale* **2012**, *4*, 1208–19.
- [4] L. C. Grabow, in *Comput. Catal.* (Eds.: A. Asthagiri, M.J. Janik), RSC Publishing, **2013**, pp. 1–58.
- [5] C. A. Wolcott, A. J. Medford, F. Studt, C. T. Campbell, *J. Catal.* **2015**, *330*, 197–207.
- [6] F. Abild-Pedersen, J. Greeley, F. Studt, J. Rossmeisl, T. Munter, P. Moses, E. Skúlason, T. Bligaard, J. K. Nørskov, *Phys. Rev. Lett.* **2007**, *99*, 4–7.
- [7] E. M. Fernandez, P. G. Moses, A. Toftelund, H. A. Hansen, J. I. Martinez, F. Abild-Pedersen, J. Kleis, B. Hinnemann, J. Rossmeisl, T. Bligaard, et al., *Angew. Chemie Int. Ed.* **2008**, *47*, 4683–4686.
- [8] G. Jones, F. Studt, F. Abild-Pedersen, J. K. Nørskov, T. Bligaard, *Chem. Eng. Sci.* **2011**, *66*, 6318–6323.
- [9] S. Wang, B. Temel, J. Shen, G. Jones, L. C. Grabow, F. Studt, T. Bligaard, F. Abild-Pedersen, C. H. Christensen, J. K. Nørskov, *Catal. Letters* **2010**, *141*, 370–373.
- [10] H. Wang, Y. Liu, M. Li, H. Huang, H. M. Xu, R. J. Hong, H. Shen, *Optoelectron. Adv. Mater. Rapid Commun.* **2010**, *4*, 1166–1169.
- [11] J. Sehested, K. E. Larsen, A. L. Kustov, A. M. Frey, T. Johannessen, T. Bligaard, M. P. Andersson, J. K. Nørskov, C. H. Christensen, *Top. Catal.* **2007**, *45*, 9–13.
- [12] F. Studt, I. Sharafutdinov, F. Abild-Pedersen, C. F. Elkjær, J. S. Hummelshøj, S. Dahl, I. Chorkendorff, J. K. Nørskov, *Nat. Chem.* **2014**, *6*, 320–324.
- [13] Y.-H. Chin, D. Resasco, in *R. Soc. Catal.*, **1999**, pp. 1–39.
- [14] R. F. Hicks, H. Qi, M. L. Young, R. G. Lee, *J. Catal.* **1990**, *122*, 280–294.
- [15] J. G. McCarty, *Catal. Today* **1995**, *26*, 283–293.
- [16] M. Monai, T. Montini, C. Chen, E. Fonda, R. J. Gorte, P. Fornasiero, *ChemCatChem* **2015**, *7*, 2038–2046.
- [17] G. Zhu, J. Han, D. Y. Zemlyanov, F. H. Ribeiro, *J. Am. Chem. Soc.* **2004**, *126*, 9896–9897.
- [18] T. P. Senftle, A. C. T. van Duin, M. J. Janik, *ACS Catal.* **2015**, *5*, 6187–6199.
- [19] T. R. Baldwin, R. Burch, *Appl. Catal.* **1990**, *66*, 359–381.
- [20] A. Hellman, A. Resta, N. M. Martin, J. Gustafson, A. Trincherro, P. A. Carlsson, O. Balmes, R. Felici, R. Van Rijn, J. W. M. Frenken, et al., *J. Phys. Chem. Lett.* **2012**, *3*, 678–682.
- [21] E. Garbowski, C. Feumi-Jantou, N. Mouaddib, M. Primet, *Appl. Catal. A, Gen.* **1994**, *109*, 277–292.
- [22] N. Seriani, J. Harl, F. Mittendorfer, G. Kresse, *J. Chem. Phys.* **2009**, *131*, 54701.
- [23] H. H. Kan, J. F. Weaver, *Surf. Sci.* **2008**, *602*, L53–L57.
- [24] A. Trincherro, A. Hellman, H. Grönbeck, *Surf. Sci.* **2013**, *616*, 206–213.
- [25] Y.-H. Chin, C. Buda, M. Neurock, E. Iglesia, *J. Am. Chem. Soc.* **2013**, *135*, 15425–15442.
- [26] T. R. Baldwin, R. Burch, *Appl. Catal.* **1990**, *66*, 337–358.
- [27] P. Reyes, A. Figueroa, G. Pecchi, J. L. G. Fierro, *Catal. Today* **2000**, *62*, 209–217.
- [28] K. A. Goulas, S. Sreekumar, Y. Song, P. Kharidehal, G. Gunbas, P. J. Dietrich, G. R. Johnson, Y. C. Wang, A. M. Grippo, L. C. Grabow, et al., *J. Am. Chem. Soc.* **2016**, *138*, 6805–6812.
- [29] H. S. Bengaard, I. Alstrup, I. Chorkendorff, S. Ullmann, J. R. Rostrup-Nielsen, J. K. Nørskov, *J. Catal.* **1999**, *187*, 238–244.
- [30] F. Che, S. Ha, J. S. McEwen, *Appl. Catal. B Environ.* **2016**, *195*, 77–89.
- [31] G. Kresse, J. Hafner, *Phys. Rev. B* **1993**, *47*, 558–561.
- [32] G. Kresse, J. Hafner, *Phys. Rev. B* **1994**, *49*, 14251–14269.
- [33] G. Kresse, J. Furthmüller, *Phys. Rev. B* **1996**, *54*, 11169–11186.
- [34] G. Kresse, J. Furthmüller, *Comput. Mater. Sci.* **1996**, *6*, 15–50.
- [35] S. R. Bahn, K. W. Jacobsen, *Comput. Sci. Eng.* **2002**, *4*, 56–66.
- [36] P. E. Blöchl, *Phys. Rev. B* **1994**, *50*, 17953–17979.
- [37] G. Kresse, *Phys. Rev. B* **1999**, *59*, 1758–1775.
- [38] J. Perdew, J. Chevary, S. Vosko, K. Jackson, M. Pederson, D. Singh, C. Fiolhais, *Phys. Rev. B* **1993**, *48*, 4978–4978.
- [39] M. J. Gillan, *J. Phys. Condens. Matter* **1989**, *1*, 689–711.
- [40] H. J. Monkhorst, J. D. Pack, *Phys. Rev. B* **1976**, *13*, 5188–5192.
- [41] M. Digne, *J. Catal.* **2004**, *226*, 54–68.
- [42] H. Wang, L. Chen, Y. Lv, R. Ren, *Appl. Surf. Sci.* **2014**, *290*, 154–160.
- [43] L. Bengtsson, *Phys. Rev. B* **1999**, *59*, 12301–12304.
- [44] G. Henkelman, B. P. Uberuaga, H. Jónsson, *J. Chem. Phys.* **2000**, *113*, 9901.

FULL PAPER

Entry for the Table of Contents (Please choose one layout)

FULL PAPER



*Hieu A. Doan, Munish K. Sharma,
William S. Epling, and Lars C. Grabow**

Page No. – Page No.

**From Active Site Model to Real
Catalysts: Importance of the Material
Gap in the Design of Pd Catalysts for
Methane Oxidation**

Consistent trends for methane activation over a series of modified Pd/ γ -Al₂O₃ catalyst models in agreement with experimental activity measurements support the common practice of using simplified catalyst representations for computational catalyst screening.

WILEY-VCH

Accepted Manuscript